Available online at www.sciencedirect.com
ScienceDirect
Journal of Nuclear Materials 359 (2006) 227–237
journal of nuclear materials
www.elsevier.com/locate/jnucmat

Ab initio calculations of self-interstitial interaction and migration with solute atoms in bcc Fe

E. Vincent [a,b], C.S. Becquart [a,*], C. Domain [a,b]

[a] *Laboratoire de Métallurgie Physique et Génie des Matériaux, UMR 8517, Université des Science et Technologies de Lille 1, Bat. C6, F-59655 Villeneuve d'Ascq cedex, France*
[b] *Electricité de France, EDF-R&D Département MMC, Les Renardières, F-77818 Moret sur Loing cedex, France*

Received 27 April 2006; accepted 28 August 2006

Abstract

The embrittlement of pressure vessel steels under radiation has been long ago correlated with the presence of solute Cu. Indeed the atom probe and the small angle neutron scattering, principally, have revealed the formation of Cu clusters under neutron flux in reactor pressure vessel (RPV) steels and dilute FeCu alloys. Other solutes such as Ni, Mn and Si which are also found within the clusters, are now suspected to contribute to the embrittlement. The interactions of these solutes with radiation induced point defects need thus to be characterized properly in order to understand the elementary mechanisms behind the formation of these clusters. We have investigated by ab initio calculations based on the density functional theory the interactions of self-interstitials with solute atoms in dilute FeX alloys (X = Cu, Mn, Ni or Si). Different possible configurations of solute–dumbbell complexes have been studied. Their binding energies are discussed, as well as their relative stability. The migration of dumbbells with a solute atom in their vicinity was also investigated. All these results are compared to some experimental ones obtained on dilute FeX model alloys. Our results indicate that for Mn solute atoms, diffusion via an interstitial mechanism is very likely.

PACS: 61.72.Ji; 61.80.–*x*; 71.20.Be; 71.15.Mb

1. Introduction

The pressure vessels of light water reactors are made of low alloyed steels (see an example in Table 1). Under neutron irradiation, microstructural studies have showed the formation of point defect clusters and solute precipitates, concurrent with the embrittlement of the steels. These neutron radiation-induced clusters are enriched in Cu, Ni, Mn and Si solute atoms but their composition is still a debate [1]. Indeed, with small angle neutron scattering and field emission scanning transmission electron microscopy, these clusters are similar to precipitates [2,3] whereas with the tomographic

* Corresponding author. Tel.: +33 3 20 43 49 44; fax: +33 3 20 43 40 40.
E-mail address: charlotte.becquart@univ-lille1.fr (C.S. Becquart).

0022-3115/$ - see front matter © 2006 Elsevier B.V. All rights reserved.
doi:10.1016/j.jnucmat.2006.08.022

Table 1
Chemical composition (wt%) of the DAMPIERRE 2 pressure vessel steel

C	S	P	Si	Cr	Mo	Mn	Ni	Al	Co	Cu
0.16	0.008	0.008	0.19	0.24	0.55	1.25	0.74	0.009	0.01	0.07

atom probe, they appear to be more or less dilute and are sometimes called 'atmospheres' [4–7].

Understanding the diffusion mechanisms which lead to the formation of these solute clusters constitutes, today, a crucial issue. Neutron irradiation induces displacement cascades which lead to the formation of many vacancies and interstitials. The interactions between point defects and solute atoms are a key factor in the understanding of the diffusion mechanisms. However, experimental data about interactions between point defects and solute atoms are scarce and difficult to determine. Ab initio calculations are thus essential to obtain this kind of data, more especially as, today, supercells containing a large number of atoms can be used.

In a previous paper [8], ab initio calculations of solute atoms (Cu, Ni, Mn, Si) in substitution in an α-Fe lattice were performed to determine the vacancy–solute interactions as well as the solute migration energies via vacancies. In this study, ab initio results of interstitial–solute interactions, followed by solute–dumbbell complexes migration energies are presented.

2. Methodology

Our calculations have been done using the Vienna Ab initio Simulation Package VASP (version 4.6) [9,10]. They were performed in a plane-wave basis, using fully non-local Vanderbilt-type ultrasoft pseudopotentials to describe the electron–ion interaction. Exchange and correlation were described by the Perdew–Zunger functional, adding a non-local correction in the form of the generalised gradient approximation (GGA) of Perdew and Wang. All the calculations were done in the spin polarised GGA using the supercell approach with periodic boundary conditions. The pseudopotentials come from the VASP library. Brillouin zone (BZ) sampling was performed using the Monkhorst–Pack scheme. The defect calculations were done at constant volume thus relaxing only the atomic position in a supercell dimensioned with the equilibrium lattice parameter for Fe (2.8544 Å). The plane wave cut-off energy was 240 eV. Calculations with 54 (respectively 128) atom supercells were done with a BZ sampling of 125 (respectively 27) kpoints. More details on the method and in particular a comparison of full relaxation versus constant volume calculations for defects in Fe can be found in a previous work [11].

The binding energy between a Self-Interstitial Atom (SIA) and a solute atom, labelled respectively I and X, in a bcc iron matrix containing N atomic sites, is calculated as follows. The energy $E(N+I)$ of a supercell containing only the SIA is added to that $(E(N-1+X))$ of the supercell containing only the solute X in substitution. To that sum, one subtracts the energy $E(N-1+I+X)$ of the same supercell containing the SIA and the solute atom X now interacting added to that (E_{ref}) of the supercell containing no defect. Thus,

$$E_{\mathrm{b}}(I,X) = [E(N+I) + E(N-1+X)] - [E(N-1+I+X) + E_{\mathrm{ref}}]. \quad (1)$$

In this scheme, a positive binding energy indicates an attractive interaction.

The migration energy is calculated by determining the energy at the saddle point, using the nudged elastic band method [12,13]. The saddle point corresponds to the configuration where the energy is maximum for the migrating atom which is, in our case, one of the two atoms constituting the dumbbell. Four possible jumps exist for the dumbbells [14,15]: a translation jump of the dumbbell to a first nearest neighbour position, parallel to itself, a translation–rotation one to a first nearest neighbour position with a rotation of 60° of its axis, a translation-rotation one to a second nearest neighbour position with a rotation of 90° of its axis and a 60° rotation jump around its site. These four jumps are illustrated in Fig. 1.

3. Results and discussion

3.1. Self-interstitial atom–solute interaction

In the α-Fe matrix, the most stable interstitial defect is a dumbbell oriented along the ⟨1 1 0⟩ direction [14]. This result is also predicted by ab initio

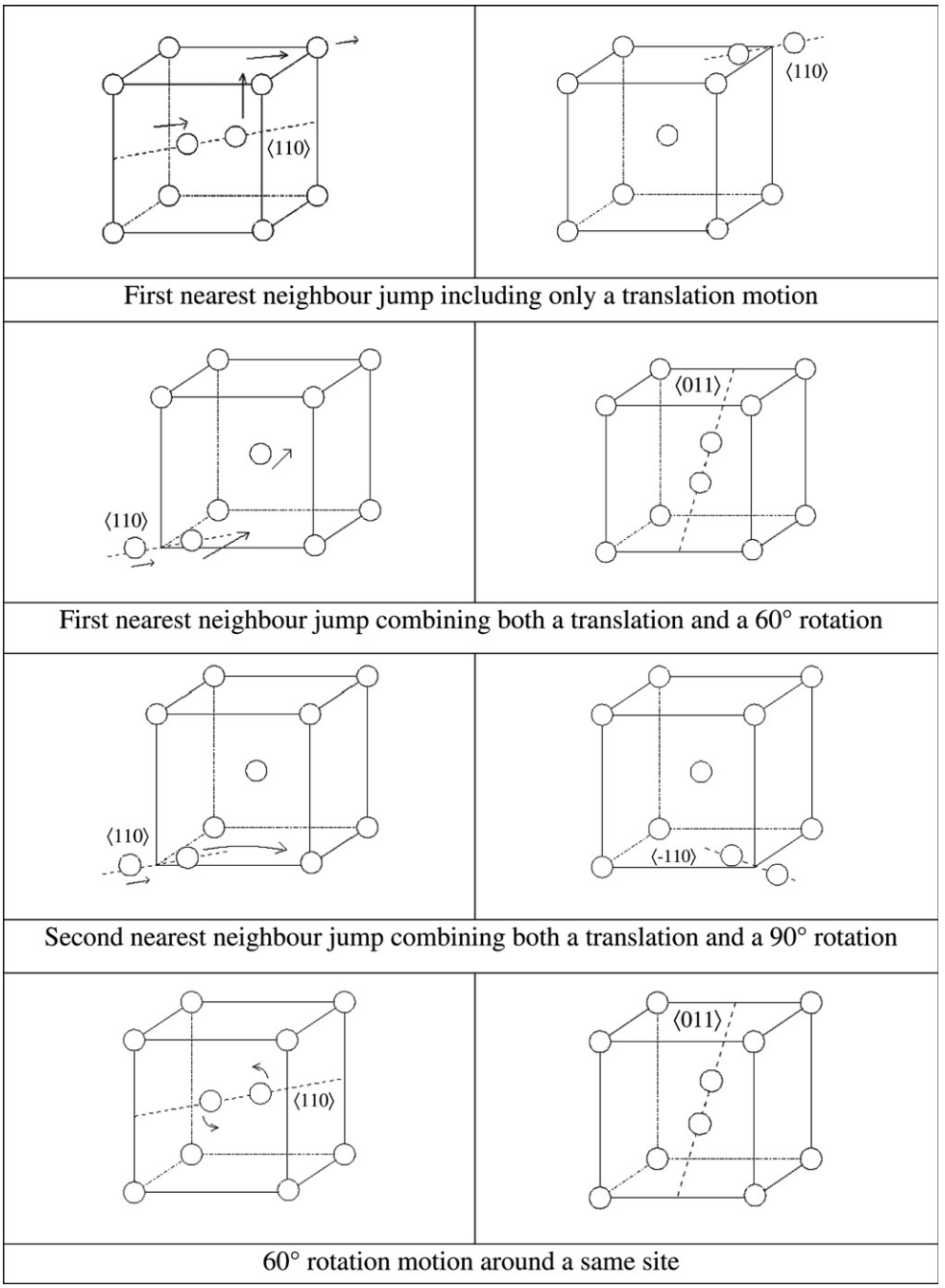

Fig. 1. Illustration of the four possible jumps for a dumbbell. The arrows indicate the motion of the dumbbell atom.

calculations [11,16]. Thus, only interactions between a ⟨1 1 0⟩ SIA dumbbell and a solute atom have been presented here in Table 3. There are three different relative positions for the solute atom up to first nearest neighbour: two for which the sites are under compression (mixed_⟨1 1 0⟩ dumbbell and $1nn^{\mathrm{Comp}}$_⟨1 1 0⟩ position) and one for which the site is under tension ($1nn^{\mathrm{Tens}}$_⟨1 1 0⟩) (Fig. 2). As the relative stability of the dumbbells is important to understand the dumbbell motion, the energy difference between a mixed ⟨1 1 1⟩ and the most stable ⟨1 1 0⟩ dumbbell configuration has also been

Table 2
Volume size-factor (Ω_{sf}, in %) of solute atoms in substitution in Fe determined by King [20] and nearest neighbour shells relaxations around the solute atoms (d_{sf}) (in % of the non-relaxed distance) determined in 128 atom supercells

Solute atom	Ω_{sf} (%)	Nearest neighbour shell relaxations		
		$d_{sf}(1nn)$ (%)	$d_{sf}(2nn)$ (%)	$d_{sf}(3nn)$ (%)
Si	−7.88	0.02	−0.77	−0.08
Mn	+4.89	0.59	−0.27	−0.10
Ni	+4.65	0.28	−0.04	−0.04
Cu	+17.53	0.93	−0.16	−0.04

1*nn* stands for first nearest neighbour and so on.

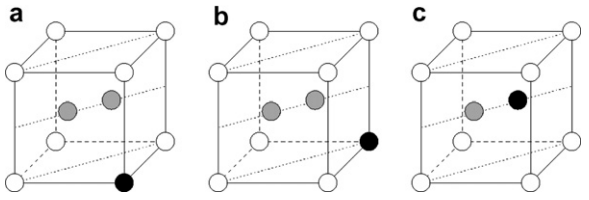

Fig. 2. ⟨1 1 0⟩_SIA–solute configurations. The black circles correspond to the solute atoms, the grey ones to the Fe atoms within the dumbbell and the white circles to the Fe atoms in the matrix, outside the dumbbell. Configuration (a) is under tension, whereas (b) and (c) are under compression.

added in the table (for pure Fe, $\Delta E_{(\langle 111\rangle-\langle 110\rangle)} = 0.80$ eV with a 54 atom supercell and 0.71 eV with a 128 atom supercell). The results indicate that the introduction of a solute atom within the dumbbells does not change their respective stabilities: i.e. the ⟨1 1 0⟩ SIA dumbbell is always the most stable interstitial.

In fcc metals [17], it has been generally accepted that oversized solutes, remaining at their lattice sites, trap self-interstitials. In contrast to this, undersized and some slightly oversized solutes combine with self-interstitials to form mixed dumbbells, displacing themselves from their lattice sites. In bcc metals, Maury showed that in alloys such as Fe–Cr [18] and Fe–Mn [19] the recovery of alloys, electron irradiated around 20 K, is enhanced compared to that in Fe between stage I_D and I_E, even though both solutes are slightly oversized: the volume size factor for Cr is +4.36% [20] and that for Mn is +4.89% [20]. They interpret these facts by the formation of mixed dumbbells moving faster than the pure Fe dumbbells at a given temperature. In FeSi alloys, these authors also acknowledge the formation of mixed dumbbells which may migrate [21]. Thus, in bcc metals, contrary to fcc ones, the stability of a SIA–solute complex does not seem to respect only a size criterion. This result is in contradiction with the simple model of Dederichs et al. [22] which predicts that whatever the structure, mixed dumbbells should be formed only for undersized solutes.

The 'size/volume' of the solute atoms, characterized by the shell relaxation of the surrounding Fe atoms obtained by ab initio calculations, is compared to their experimental volume [20] in Table 2. The calculated relaxations around the solutes are consistent with the experimental volumes. Moreover, we have calculated the solute atomic volumes in the most stable structure as well as in the bcc one (Table 4). Not surprisingly, the bigger the atomic volume in the stable structure, the bigger the atomic volume in the bcc structure. These data are in really good agreement with the experimental stable volumes at room temperature.

SIA–solute interactions have been determined for the configurations illustrated in Fig. 2, and the results are collected in Table 3. The energy differences between the results obtained with 54 and 128 atom supercells are smaller than 0.07 eV and remain within the uncertainty of these calculations (≈0.1 eV). For each solute, the relative stability of the three configurations studied is discussed.

According to our calculations (Table 3) and for the configurations explored (Fig. 2), no interaction between a SIA and Ni seems to exist. For the other solutes, an attractive interaction, which increases

Table 3
⟨1 1 0⟩ SIA–solute (Si, Mn, Ni and Cu) binding energies (eV) obtained with 54- and 128-atom supercells, for the configurations of Fig. 2. For Mn, the antiferro-magnetic (af) or ferro-magnetic (f) states are indicated. The last line corresponds to the energy difference between the mixed_⟨1 1 1⟩ configuration and the most stable ⟨1 1 0⟩ SIA–solute complex

Energy (eV)	Si		Mn		Ni		Cu	
Supercell size (atoms)	54	128	54	128	54	128	54	128
$1nn^{Tens}$_⟨1 1 0⟩	−0.26	−0.23	−0.36 f	−0.36 f	−0.14	−0.13	0.06	0.07
$1nn^{Comp}$_⟨1 1 0⟩	0.24	0.27	0.09 af	0.10 af	−0.06	−0.06	−0.03	−0.01
mixed_⟨1 1 0⟩	−0.05	0.01	0.36 af	0.37 af	−0.36	−0.36	−0.53	−0.46
$\Delta E_{(\text{mixed\_}\langle 1\,1\,1\rangle-\langle 1\,1\,0\rangle)}$ (eV)	0.66	0.52	0.66	0.59	0.78	0.75	0.85	0.73

Table 4
Atomic volumes in the stable and in the bcc structure of solutes

Structure	Si Diamond	Mn Complex cubic	Ni fcc	Cu fcc	Fe bcc
First neighbour distance (nm)	0.235	0.224	0.249	0.256	0.248
Ω (10^{-2} nm^3)	2.001	1.221	1.090	1.176	1.182
Ω (10^{-2} nm^3) (ab initio)	2.030		1.095	1.207	1.163
Ω (10^{-2} nm^3) bcc (ab initio)	1.485	1.197	1.104	1.210	1.163

The Mn atomic volume has not been calculated in the complex cubic structure. Experimental stable structures at room temperature of the solute atoms as well as Fe and the corresponding first nearest neighbour distances and experimental atomic volumes [36].

from Cu to Si to Mn, appears. Mn behaves differently than the other solutes: it is the only solute whose most stable configuration is a mixed $\langle 1\,1\,0\rangle$ dumbbell. The configuration is very stable as the binding energy is very high (0.37 eV). For the other solutes, the mixed dumbbell configuration appears either really unfavourable (Ni and Cu solute atoms) or neutral. These effects can be explained by the shell relaxation induced by each mixed dumbbell. Compared to the distance between the two Fe atoms in the pure Fe dumbbell (0.191 nm), the distance between the Fe and Mn atoms in the dumbbell is slightly reduced (−0.7%). The strain on the neighbouring Fe atoms induced by the presence of the dumbbell is thus decreased when one element of the dumbbell is a Mn atom. On the other hand, for Cu, Ni and Si, the Fe–solute distances in the mixed dumbbells are greater than the Fe–Fe distance in the pure iron dumbbell. Indeed, it is increased by 6% for Ni and by 8% for Si and Cu.

Si establishes an attractive bond with a $\langle 1\,1\,0\rangle$ dumbbell only when it is in the $1nn^{\mathrm{Comp}}$ configuration. Being an undersized solute atom, its position in the plane containing the dumbbell relieves partly the strain induced by the later. Nevertheless, in our calculations, the mixed dumbbell interaction appears neutral maybe because it dislikes being in too compact of a structure with a high co-ordinance as can be deduced from the data of Table 4.

Ni, even if it is a bit oversized as compared to Fe, is one of the smallest solute atoms studied both in its stable structure and in the bcc one (see Table 4). The most favourable position is the $1nn^{\mathrm{Comp}}$ one but, because of the low value of the binding energy and the uncertainties of the calculations, it is difficult to conclude on the attractive or repulsive character of the bond. The mixed dumbbell, the most compact configuration, is clearly the most unfavourable position.

For Mn, the most stable configuration is the mixed_$\langle 1\,1\,0\rangle$ dumbbell. An attractive binding energy seems to exist also in the $1nn^{\mathrm{Comp}}$ configuration. These results indicate that although Mn is an oversized solute atom, it tends to adopt compact configurations. This is in agreement with the short experimental first nearest neighbour distance of the Mn complex cubic structure. A high positive Mn–SIA interaction (0.37 eV), higher than the Mn–vacancy one (ab initio calculations: 0.12 eV ($1nn$), 0.07 eV ($2nn$) [8]; experience: 0.15 eV [23]) can explain Wirth results [24] who observes a lack of vacancy cluster formation and the formation of smaller solute clusters, in irradiated FeCuMn ternary alloys as compared to FeCu binary ones [25]. Indeed these interactions indicate a preference for Mn to bind to SIAs than to vacancies.

Finally, Cu being the most oversized solute (Table 2) is likely to join a site which is not too compressed by the lattice surrounding. Table 3 indicates weak interactions of a Cu solute atom with a SIA ($1nn^{\mathrm{Comp}}$ configuration and $1nn^{\mathrm{Tens}}$ configuration) whose values are within the uncertainties of the method. It is thus difficult to conclude. The formation of a mixed dumbbell appears to be really unfavourable, in agreement with the first nearest neighbour distance in fcc Cu being the largest in Table 4. With the Fe–Cu many-body interatomic potential of Ackland [26], Marian et al. [27] also found negative binding energies for mixed dumbbells.

To summarize, Mn seems to be the solute atom which interacts the most with the SIA. Therefore, it is the most likely to migrate through an interstitial mechanism.

3.2. SIA–solute migration

Le Claire [28] showed that impurities diffuse by a vacancy mechanism when their diffusion rates are comparable with the host self-diffusion rate. When the impurity diffusion rate greatly exceeds that of self-diffusion, the vacancy mechanism is untenable

and diffusion is believed to be dominated by some form of interstitial migration [28]. Under irradiation, many interstitials are created and some solutes may migrate by an interstitial mechanism [29]. It is thus important to study this kind of motion. In Section 2, the four different possible jumps [14,15] (Fig. 1) were described. Nevertheless, solute transport can only occur if mixed dumbbells form and migrate [29]. More precisely, solute transport can occur when the solute atom of a mixed dumbbell initiates a jump to one of the nearest sites, that is to say undergoes one of the jumps illustrated in Fig. 3(a.1), (a.2) or (b.1).

The migration energies necessary to estimate whether these different jumps can occur or not were determined by ab initio calculations using 54-atom supercells. During the migration involving a translation without rotation, the $\langle 1\,1\,0\rangle$ dumbbell becomes a $\langle 1\,1\,1\rangle$ dumbbell when the migrating atom is at the saddle point. Consequently, the corresponding migration energy is simply given by the difference of energy of the $\langle 1\,1\,1\rangle$ dumbbell configuration and of the $\langle 1\,1\,0\rangle$ dumbbell one. Similarly, for the second nearest neighbour jumps (Fig. 3(b)), the migrating atom passes through a tetrahedral site. Thus, the mixed to mixed migration energy, which corresponds to the jump illustrated in Fig. 3(b.1), is simply given by the difference of energy of the solute atom in a tetrahedral configuration and of the mixed_$\langle 1\,1\,0\rangle$ dumbbell one. For the other mechanisms, the nudged elastic band method was applied. In Table 5, as a preliminary result, the dumbbell migration energies in pure α-Fe, calculated with a 54-atom supercell and 125 kpoints are compared

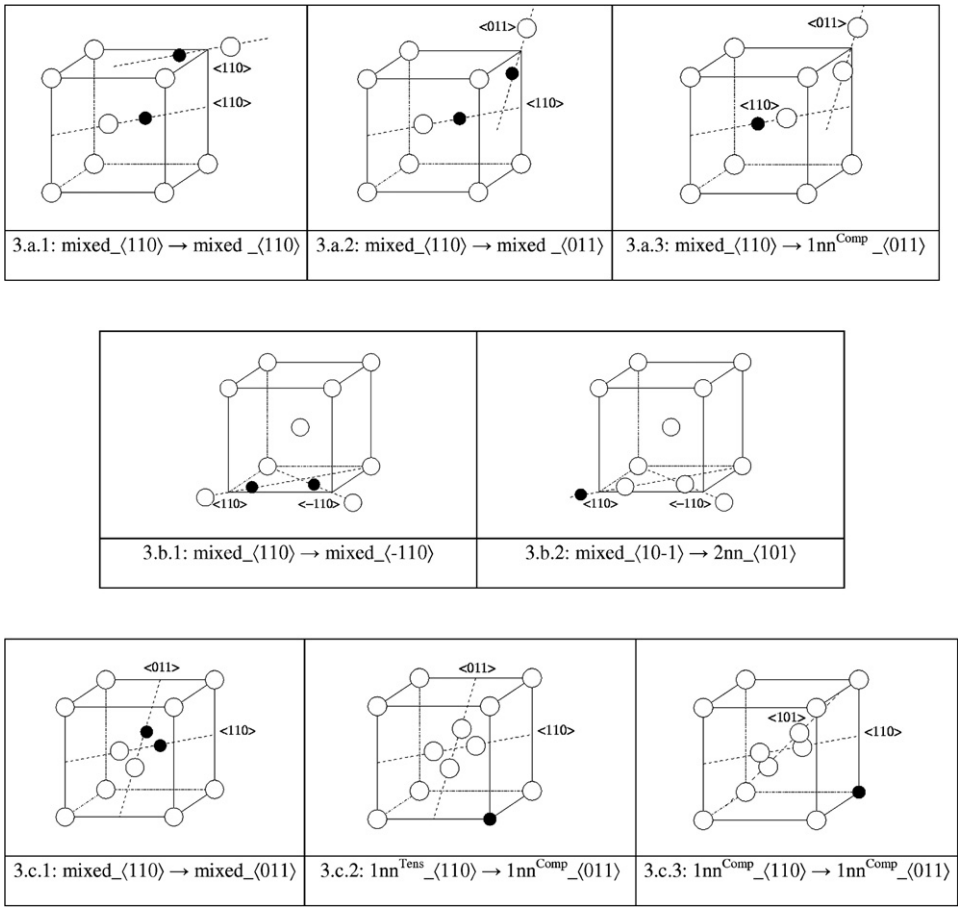

Fig. 3. Possible jump configurations for a dumbbell in a vicinity of a solute atom (black circle). The axis of the dumbbell is written in brackets and the configuration names correspond to the ones in Fig. 2. In the first line, (a.1) corresponds to a jump involving only a translation, (a.2) and (a.3) to two translation–rotation jumps. The jumps represented in (a.1) and (a.2) lead to solute transport. In the second line, (b.1) and (b.2) correspond to two second neighbour jumps. They include a translation and a 90° rotation. Only the jump in (b.1) leads to solute transport. In the last line, (c.1), (c.2) and (c.3) correspond to three rotation jumps. They cannot lead to solute transport.

Table 5
Dumbbell migration energies obtained in a pure α-Fe lattice calculated in this work with a 54-atom supercell and 125 kpoints. The results are compared with those of Fu et al. [16] obtained with the SIESTA code and with a 128-atom supercell and 27 kpoints, as well as with those of Johnson obtained with an empirical potential in [30]

Migration energy (eV)	This work	[16]	[30]
E_{mig} ($\langle 1\,1\,0\rangle \rightarrow \langle 1\,1\,0\rangle$ via $\langle 1\,1\,1\rangle$)	0.80	0.78	
E_{mig} ($\langle 1\,1\,0\rangle \rightarrow \langle 0\,1\,1\rangle$)	0.37	0.34	0.33
E_{mig} ($\langle 1\,1\,0\rangle \rightarrow \langle 1\,-1\,0\rangle$)	0.57	0.5	
E_{rot} ($\langle 1\,1\,0\rangle \rightarrow \langle 0\,1\,1\rangle$)	0.63	0.56	0.33

to that of Fu et al. [16] obtained with the SIESTA code using supercells of 128 atoms and 27 kpoints. The results are in good agreement, with an energy difference inferior to the ab initio calculations uncertainty and the relative stabilities are the same in each series of calculations. This comparison shows that the calculation is well converged with respect to the supercell size. Moreover, each result indicates that the jump combining a rotation and a translation is the most probable one. Some values are also compared to the results of Johnson [30], who described an α-Fe crystal using an empirical potential. He found the same value (0.33 eV) for the migration-60° rotation motion and the pure 60° rotation one. Our results are only consistent with the migration-rotation jump. Experimentally, Takaki et al. [31] found an energy of 0.3 eV for the migration of the Fe–Fe dumbbell.

The barriers for the different possible jumps studied (illustrated in Fig. 3), are collected in Table 6 for each solute atom, and for sake of clarity the barriers are plotted in Fig. 4.

For Si (Table 6a), the energetic barriers to form mixed dumbbells, represented in Fig. 3(a.3) and (b.2), are globally not too high since they are below the barrier of the most favourable pure iron dumbbell jump (0.37 eV). However, one of the barriers to dissociate the mixed dumbbell is very low (Fig. 3(a.3)). As a consequence, even if a Si atom succeeds in forming a mixed dumbbell (which is a non-stable configuration (Table 3)), its probability to migrate through this configuration is very low. Furthermore, the $1nn^{Comp}\_\langle 1\,1\,0\rangle$ configuration is very stable. The transport of Si solute atoms via interstitials, which can be possible, only if mixed dumbbells are formed and migrate, does not seem to be plausible.

The Fe–Ni mixed dumbbell configuration is unstable and the mixed to mixed migration energies (Fig. 3(a.1), (a.2) and (b.1)) are high (Table 6b). Moreover, the energetic barriers which enable to dissociate a mixed dumbbell, represented in Fig. 3(a.3) and (b.2), are favourable. Furthermore, they are lower than the barriers that a solute atom has to jump over to form a mixed dumbbell. For instance, the energy needed to have a $1nn^{Comp}\_\langle 1\,1\,0\rangle$ configuration from a mixed dumbbell one equals 0.13 eV as compared to 0.45 eV to be in a mixed dumbbell configuration from a $1nn^{Comp}\_\langle 1\,1\,0\rangle$ one. To summarize, since the Fe–Ni mixed dumbbell configuration is unstable and the migration energies which lead to dissociate a mixed dumbbell are more favourable than the ones which lead to the formation or the migration of mixed dumbbells, Ni solute atoms are not supposed to migrate through an interstitial mechanism.

For Mn, which is the only solute for which the mixed dumbbell is a really favourable configuration, the energy of the mixed to mixed dumbbell migration, combining a translation and a rotation (Fig. 3(a.2)), is low (Table 6c) and comparable to the corresponding one of iron. The energetic barriers that a pure Fe dumbbell has to jump over to form a mixed dumbbell are lower than that of the most stable jump of a pure iron dumbbell (0.37 eV). Moreover, the barriers, which enable to transform a mixed dumbbell in a pure Fe dumbbell, are higher than that of the most stable mixed to mixed jump (0.34 eV). As to the rotation of a mixed dumbbell (Fig. 3(c.1)), it does not require much energy. Consequently, in presence of Mn, Fe–Mn mixed dumbbells are likely to form and to migrate in the three space directions as they are able to reorient themselves. This result appears clearly in Fig. 4. Thus, the transport of Mn solute atoms via dumbbells seems to be possible. Due to the low energy of the mixed to mixed migration (Fig. 3(a.2)) and the fact that the mixed dumbbell configuration is very stable, the Mn diffusion could be a long ranged process.

The Fe–Cu mixed dumbbell configuration is more unstable than the Fe–Ni one. Nevertheless, some of the mixed to mixed migration (Fig. 3(a.1) and (a.2)) energies, appearing in Table 6d, are low. On the other hand, the lowest migration energies, whose values are close to zero, are the ones that lead to the dissociation of the mixed dumbbell (Fig. 3(a.3) and (b.2)). Consequently, even if the mixed to mixed migration energies are low, the dissociation of the mixed dumbbell is so favourable and the interaction of the mixed dumbbell is so

Table 6
Dumbbell migration energies in the vicinity of a solute atom (Cu, Ni, Si or Mn)

	Figure	Energy (eV)
(a) Si		
E_{mig} (mixed_⟨1 1 0⟩ → mixed_⟨1 1 0⟩ via ⟨1 1 1⟩)	Fig. 3(a.1)	0.37
E_{mig} (mixed_⟨1 1 0⟩ → mixed_⟨0 1 1⟩)	Fig. 3(a.2)	0.52
E_{mig} (mixed_⟨1 1 0⟩ → $1nn^{Comp}$_⟨0 1 1⟩)	Fig. 3(a.3)	0.06
E_{mig} ($1nn^{Comp}$_⟨0 1 1⟩ → mixed_⟨1 1 0⟩)	Fig. 3(a.3)	0.35
E_{mig} (mixed_⟨1 1 0⟩ → mixed_⟨−1 1 0⟩)	Fig. 3(b.1)	0.67
E_{mig} (mixed_⟨1 1 0⟩ → 2*nn*_⟨−1 1 0⟩)	Fig. 3(b.2)	0.26
E_{mig} (2*nn*_⟨−1 1 0⟩ → mixed_⟨1 1 0⟩)	Fig. 3(b.2)	0.14
E_{rot} (mixed_⟨1 1 0⟩ → mixed_⟨0 1 1⟩)	Fig. 3(c.1)	0.48
E_{rot} ($1nn^{Tens}$_⟨1 1 0⟩ → $1nn^{Comp}$_⟨0 1 1⟩)	Fig. 3(c.2)	0.33
E_{rot} ($1nn^{Comp}$_⟨0 1 1⟩ → $1nn^{Tens}$_⟨1 1 0⟩)	Fig. 3(c.2)	0.84
E_{rot} ($1nn^{Comp}$_⟨1 1 0⟩ → $1nn^{Comp}$_⟨0 1 1⟩)	Fig. 3(c.3)	0.36
(b) Ni		
E_{mig} (mixed_⟨1 1 0⟩ → mixed_⟨1 1 0⟩ via ⟨1 1 1⟩)	Fig. 3(a.1)	0.46
E_{mig} (mixed_⟨1 1 0⟩ → mixed_⟨0 1 1⟩)	Fig. 3(a.2)	0.45
E_{mig} (mixed_⟨1 1 0⟩ → $1nn^{Comp}$_⟨0 1 1⟩)	Fig. 3(a.3)	0.13
E_{mig} ($1nn^{Comp}$_⟨0 1 1⟩ → mixed_⟨1 1 0⟩)	Fig. 3(a.3)	0.45
E_{mig} (mixed_⟨1 1 0⟩ → mixed_⟨−1 1 0⟩)	Fig. 3(b.1)	0.84
E_{mig} (mixed_⟨1 1 0⟩ → 2*nn*_⟨−1 1 0⟩)	Fig. 3(b.2)	0.23
E_{mig} (2*nn*_⟨−1 1 0⟩ → mixed_⟨1 1 0⟩)	Fig. 3(b.2)	0.45
E_{rot} (mixed_⟨1 1 0⟩ → mixed_⟨0 1 1⟩)	Fig. 3(c.1)	0.36
E_{rot} ($1nn^{Tens}$_⟨1 1 0⟩ → $1nn^{Comp}$_⟨0 1 1⟩)	Fig. 3(c.2)	0.52
E_{rot} ($1nn^{Comp}$_⟨0 1 1⟩ → $1nn^{Tens}$_⟨1 1 0⟩)	Fig. 3(c.2)	0.60
E_{rot} ($1nn^{Comp}$_⟨1 1 0⟩ → $1nn^{Comp}$_⟨0 1 1⟩)	Fig. 3(c.3)	0.45
(c) Mn		
E_{mig} (mixed_⟨1 1 0⟩ → mixed_⟨1 1 0⟩ via ⟨1 1 1⟩)	Fig. 3(a.1)	0.66
E_{mig} (mixed_⟨1 1 0⟩ → mixed_⟨0 1 1⟩)	Fig. 3(a.2)	0.34
E_{mig} (mixed_⟨1 1 0⟩ → $1nn^{Comp}$_⟨0 1 1⟩)	Fig. 3(a.3)	0.49
E_{mig} ($1nn^{Comp}$_⟨0 1 1⟩ → mixed_⟨1 1 0⟩)	Fig. 3(a.3)	0.22
E_{mig} (mixed_⟨1 1 0⟩ → mixed_⟨−1 1 0⟩)	Fig. 3(b.1)	0.53
E_{mig} (mixed_⟨1 1 0⟩ → 2*nn*_⟨−1 1 0⟩)	Fig. 3(b.2)	0.80
E_{mig} (2*nn*_⟨−1 1 0⟩ → mixed_⟨1 1 0⟩)	Fig. 3(b.2)	0.04
E_{rot} (mixed_⟨1 1 0⟩ → mixed_⟨0 1 1⟩)	Fig. 3(c.1)	0.45
E_{rot} ($1nn^{Tens}$_⟨1 1 0⟩ → $1nn^{Comp}$_⟨0 1 1⟩)	Fig. 3(c.2)	0.54
E_{rot} ($1nn^{Comp}$_⟨0 1 1⟩ → $1nn^{Tens}$_⟨1 1 0⟩)	Fig. 3(c.2)	0.99
E_{rot} ($1nn^{Comp}$_⟨1 1 0⟩ → $1nn^{Comp}$_⟨0 1 1⟩)	Fig. 3(c.3)	0.28
(d) Cu		
E_{mig} (mixed_⟨1 1 0⟩ → mixed_⟨1 1 0⟩ via ⟨1 1 1⟩)	Fig. 3(a.1)	0.26
E_{mig} (mixed_⟨1 1 0⟩ → mixed_⟨0 1 1⟩)	Fig. 3(a.2)	0.32
E_{mig} (mixed_⟨1 1 0⟩ → $1nn^{Comp}$_⟨0 1 1⟩)	Fig. 3(a.3)	0.00
E_{mig} ($1nn^{Comp}$_⟨0 1 1⟩ → mixed_⟨1 1 0⟩)	Fig. 3(a.3)	0.50
E_{mig} (mixed_⟨1 1 0⟩ → mixed_⟨−1 1 0⟩)	Fig. 3(b.1)	0.59
E_{mig} (mixed_⟨1 1 0⟩ → 2*nn*_⟨−1 1 0⟩)	Fig. 3(b.2)	0.05
E_{mig} (2*nn*_⟨−1 1 0⟩ → mixed_⟨1 1 0⟩)	Fig. 3(b.2)	0.33
E_{rot} (mixed_⟨1 1 0⟩ → mixed_⟨0 1 1⟩)	Fig. 3(c.1)	0.32
E_{rot} ($1nn^{Tens}$_⟨1 1 0⟩ → $1nn^{Comp}$_⟨0 1 1⟩)	Fig. 3(c.2)	0.58
E_{rot} ($1nn^{Comp}$_⟨0 1 1⟩ → $1nn^{Tens}$_⟨1 1 0⟩)	Fig. 3(c.2)	0.49
E_{rot} ($1nn^{Comp}$_⟨1 1 0⟩ → $1nn^{Comp}$_⟨0 1 1⟩)	Fig. 3(c.3)	0.62

The migrations correspond to a translation, a translation combined with a rotation or a pure rotation. They were obtained by ab initio calculations with a 54-atom supercell and 125 kpoints.

repulsive, that the diffusion of Cu solute atoms via interstitials does not seem plausible either. This result appears clearly in Fig. 4.

In conclusion, the calculations of specific migration and rotation energies of a dumbbell in the vicinity of a solute atom lead to conclude that the

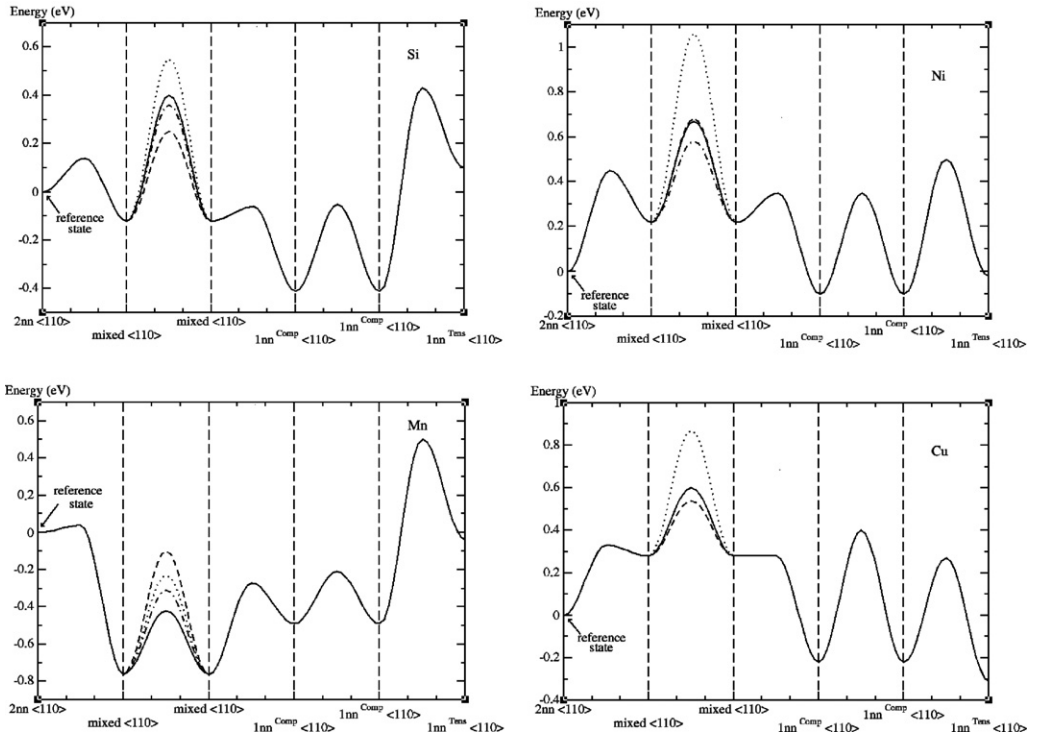

Fig. 4. Dumbbell migration barriers in the vicinity of a solute atom (Si, Ni, Mn or Cu). For the mixed to mixed dumbbell migration, the four possible jumps are represented: the first nearest neighbour jump combining a translation and a rotation (Fig. 3(a.2)) is represented by the continuous line, the first nearest neighbour translation jump (Fig. 3(a.1)) by the dashed line, the second nearest neighbour jump combining a translation and a rotation (Fig. 3(b.1)) by the dotted line and the rotation jump (Fig. 3(c.1)) is represented by the dashed–dotted line.

transport of solute atoms via an interstitial mechanism is plausible only for Mn.

Some experimental results dealing with the formation and the migration of solute–dumbbell complexes are available. Experiments consist of the irradiation at low temperatures of Fe–X binary alloys (X = Cu, Mn, Ni, Si, Au, Cr, ...) and of the analysis of the recovery of the irradiated materials during isochronal annealings by electrical resistivity, magnetic after-effect or internal friction measurements. Maury et al. [19,21,32] electron irradiated Fe–X (X = Cu, Ni, Mn and Si) binary alloys which they analysed by electrical resistivity measurements. Abe and Kuramoto [33] made the same experiments for the Fe–Si binary alloy. Hasiguti [34] neutron irradiated Fe–Ni binary alloys analysed then using internal friction techniques. Blythe et al. [35] electron and/or neutron irradiated Fe–X (X = Cu, Ni, Mn and Si) binary alloys which were examined by magnetic after-effect measurements. These techniques can indeed bring information about the trapping of SIAs, the formation (or not) of mixed dumbbells, the possible migration of solute–dumbbell complexes and the temperature range in which these events take place.

Our results for Si indicate that SIAs can be strongly trapped by these atoms when they are in the $1nn^{\mathrm{Comp}}\_\langle 1\,1\,0\rangle$ position which is in good agreement with the conclusion of Blythe et al. [35]. As to the formation of mixed dumbbells, our calculations indicate that it is a neutral configuration, while Maury et al. [21] and Abe and Kuramoto [33] both interpret their results by the formation of mixed dumbbells.

Maury et al. [19,32] conclude about the trapping of interstitials by Ni atoms. It is difficult to obtain a clear opinion about the existence of this kind of trapping from our results because of the very low absolute value of the binding energy obtained in the $1nn^{\mathrm{Comp}}\_\langle 1\,1\,0\rangle$ compared to the calculation uncertainty. Furthermore, Hasiguti concludes about the trapping of interstitials by Ni atoms while obtaining a binding energy of only 0.03 eV between the two elements. This, we believe, is incompatible

with a strong binding energy. Nevertheless, the results of our calculations indicate also that the Fe–Ni mixed dumbbell is very unstable, which is not consistent with the interpretations of Maury et al. [19,32].

Our results for Mn are in agreement both with the data obtained by Maury et al. [19,32] and by Blythe et al. [35]. The strong interaction we obtain for the Fe–Mn mixed dumbbell associated with low barriers for its migration is coherent with a high probability for its formation and its migration, with a mobility at least comparable with that of a SIA, as constitute the main conclusions of Maury et al.

Blythe et al. [35] conclude about a strongly reduced trapping of the dumbbells by Cu atoms as compared to the FeSi system. From our calculations, similarly to the case of the Fe–Ni system, the absolute values of the binding energies obtained are too close to zero to be able to conclude unequivocally on the existence or not of trapping. In that case also, Maury et al. [32] interpret the resistivity curves by the formation of mixed dumbbells, while our calculations predict that such a configuration is not stable.

Some discrepancies exist between our calculations and electrical resistivity recovery measurements. They can be due to uncertainties existing in each method. On the one hand, ab initio calculations uncertainty on binding energies is about 0.1 eV. On the other hand, electrical resistivity recovery is an experimental technique in which the interpretation of the various peaks and stages is not so obvious and different scenarios can be associated to the resistivity changes. SIAs trapping certainly takes place as it involves the disappearance of the peak which is commonly admitted to correspond to the $\langle 1\,1\,0\rangle$ dumbbell motion in pure iron. The mixed dumbbell migration is admitted to rely both on the amplitude growth and the position shift towards lower temperatures of the recovery peak I_E when the solute concentration increases. However, the temperature shift can be difficult to identify as it is of only a few degrees for a solute concentration going from 50 to 400 at. ppm.

In a previous work [8], we had determined the interactions between Cu, Ni, Si, Mn and a vacancy in an α-Fe matrix. Our results agreed with experimental data and indicated that for Ni, Cu and Si solutes, diffusion via a vacancy mechanism could be efficient. In this work, a careful examination of the interaction of the SIA with the same solute elements seems to indicate that for Mn, transport through a self-interstitial type mechanism is the most probable.

4. Conclusions

Using ab initio approach, we had previously established that for Cu, Ni and Si, diffusion in α-Fe via a vacancy mechanism is very plausible, in agreement with experimental results.

In this work, ab initio calculations of the binding and the migration energies of solute–dumbbell complexes have been performed in a dilute FeX (X = Cu, Ni, Mn, Si) alloy. For Ni and Cu because of the low values obtained, it is difficult to deduce from our calculations, whether the trapping of SIAs by these solutes can take place or not. On the other hand, the formation of mixed dumbbells is clearly not favourable. For Si, these new results indicate that trapping of SIAs in bcc Fe by this solute can take place, however the formation of mixed dumbbells can not be firmly established. For Mn, the results of these calculations lead to think, that solute transport in α-Fe through an interstitial mechanism is very likely.

Acknowledgement

The authors wish to thank F. Maury for very interesting and kind discussions. This work has been performed within the European PERFECT project (FI6O-CT-2003-508840) which has sponsored this study. This research has been done using the CRI supercomputer of the USTL supported by the Fonds Européens de Développement Régional, as well as the CEA CCRT supercomputers in the framework of an EDF-CEA contract.

References

[1] M.K. Miller, B.D. Wirth, G.R. Odette, Mater. Sci. Eng. A353 (2003) 133.
[2] J.T. Buswell, W.J. Phythian, R.J. McElroy, S. Dumbill, P.H.N. Ray, J. Mace, R.N. Sinclair, J. Nucl. Mater. 225 (1995) 196.
[3] B.D. Wirth, PhD thesis, University of California, Santa Barbara, 1995.
[4] P. Auger, P. Pareige, M. Akamatsu, J.C. Van Duysen, J. Nucl. Mater. 211 (1994) 194.
[5] B. Radiguet, PhD thesis, Université de Rouen, 2004.
[6] M.K. Miller, P. Pareige, Mat. Res. Soc. Symp. 650 (2001) R6.1.1.
[7] M.K. Miller, M.G. Burke, J. Nucl. Mater. 195 (1992) 68.
[8] E. Vincent, C.S. Becquart, C. Domain, Nucl. Instr. and Meth. B 228 (2005) 137.

[9] G. Kresse, J. Hafner, Phys. Rev. B 47 (1993) R558; G. Kresse, J. Hafner, Phys. Rev. B 49 (1994) 14251.
[10] G. Kresse, J. Furthmüller, Comput. Mater. Sci. 6 (1996) 15.
[11] C. Domain, C.S. Becquart, Phys. Rev. B 65 (2002) 024103.
[12] G. Mills, H. Jonsson, G.K. Schenter, Surf. Sci. 324 (1995) 305.
[13] H. Jonsson, G. Mills, K.W. Jacobsen, Nudged elastic band method for finding minimum energy paths of transitions, in: B.J. Berne, G. Ciccotti, D.F. Coker (Eds.), Classical and Quantum Dynamics in Condensed Phase Simulations, World Scientific, 1998.
[14] P. Ehrhart, K.H. Robrock, H.R. Schober, in: R.A. Johnson, A.N. Orlov (Eds.), Part 1 of volume 13: Physics of radiation effects in crystals, in: V.M. Agranovich, A.A. Maradudin (Eds.), Modern problems in condensed matter sciences, North Holland, Amsterdam, Oxford, New York, Tokyo, 1986.
[15] J.L. Bocquet, Phil. Mag. A 63 (1991) 157.
[16] C.-C. Fu, F. Willaime, P. Ordejón, Phys. Rev. Lett. 92 (2004) 175503.
[17] H. Wollenberger, J. Nucl. Mater. 69&70 (1978) 362.
[18] F. Maury, P. Lucasson, A. Lucasson, F. Faudot, J. Bigot, J. Phys. F: Met. Phys. 17 (1987) 1143.
[19] F. Maury, A. Lucasson, P. Lucasson, Y. Loreaux, P. Moser, J. Phys. F: Met. Phys. 16 (1986) 523.
[20] H.W. King, J. Mater. Sci. 1 (1966) 79.
[21] F. Maury, A. Lucasson, P. Lucasson, P. Moser, Y. Loreaux, J. Phys. F: Met. Phys. 15 (1985) 1465.
[22] P.H. Dederichs, C. Lehmann, H.R. Schober, A. Scholz, R. Zeller, J. Nucl. Mater. 69&70 (1978) 176.
[23] A. Möslang, E. Albert, E. Recknagel, A. Weidinger, Hyperfine Interact. 15-16 (1983) 409.
[24] B.D. Wirth, private communication.
[25] S.C. Glade, B.D. Wirth, G.R. Odette, P. Asoka-Kumar, P.A. Sterne, R.H. Howell, Phil. Mag. 85 (2005) 629.
[26] G.J. Ackland, D.J. Bacon, A.F. Calder, T. Harry, Phil. Mag. A 75 (1997) 713.
[27] J. Marian, B.D. Wirth, J.M. Perlado, G.R. Odette, T. Diaz de la Rubia, Phys. Rev. B 64 (2001) 094303.
[28] A.D. Le Claire, J. Nucl. Mater. 69&70 (1978) 70.
[29] P. Lucasson, F. Maury, A. Lucasson, Radiat. Eff. Lett. 85 (1985) 219.
[30] R.A. Johnson, Phys. Rev. 134 (1964) A1329.
[31] S. Takaki, J. Fuss, H. Kugler, U. Dedek, H. Schultz, Rad. Eff. 79 (1983) 87.
[32] F. Maury, A. Lucasson, P. Lucasson, P. Moser, F. Faudot, J. Phys.: Condens. Matter. 2 (1990) 9291.
[33] H. Abe, E. Kuramoto, J. Nucl. Mater. 271-272 (1999) 209.
[34] R.R. Hasiguti, Nucl. Metall. 18 (1973) 1.
[35] H.J. Blythe, H. Kronmüller, A. Seeger, F. Walz, Phys. Status Solidi (a) 181 (2000) 233.
[36] C. Kittel, Introduction to Solid State Physics, 6th Ed., Wiley, New York, 1987.